CHAPTER III

VICKERS-PRODUCED DEFORMATION / FRACTURE PATTERNS

Before dealing with the investigation of surface damages of cattle bone material produced by indenting with a standard Vickers diamond pyramid indenter (square base with an angle of 136° between opposite faces of the pyramid and 148° between the pyramid edges), we will first give a broad perspective of the various Vickers-produced damage observed in glasses and many ceramics along with their fracture mechanics formulations. However, we will begin this chapter with the outline of theoretical framework of brittle fracture in order to provide some appreciation of the basic fracture mechanics involved. The studies in this chapter need the important experimental equipments as shown in FIgs. A. 6 to A. 9.

3.1 Background Theory of Indentation Fracture Mechanics

3.1.1 Theoretical Framework of Brittle Fracture

To outline the mechanics of crack growth in brittle solids, we begin with a picture of a slitlike crack of length c in linear elastic continuum which is subjected to applied load L at its outer boundary. In terms of a polar coordinated system in Fig. 3.1, the solutions for the near stress field about the crack tip σ_{ij} can be expressed in the form

$$\sigma_{ij} = K(L,c)(2\pi r)^{-1/2} f_{ij}(\theta) \qquad (3.1)$$

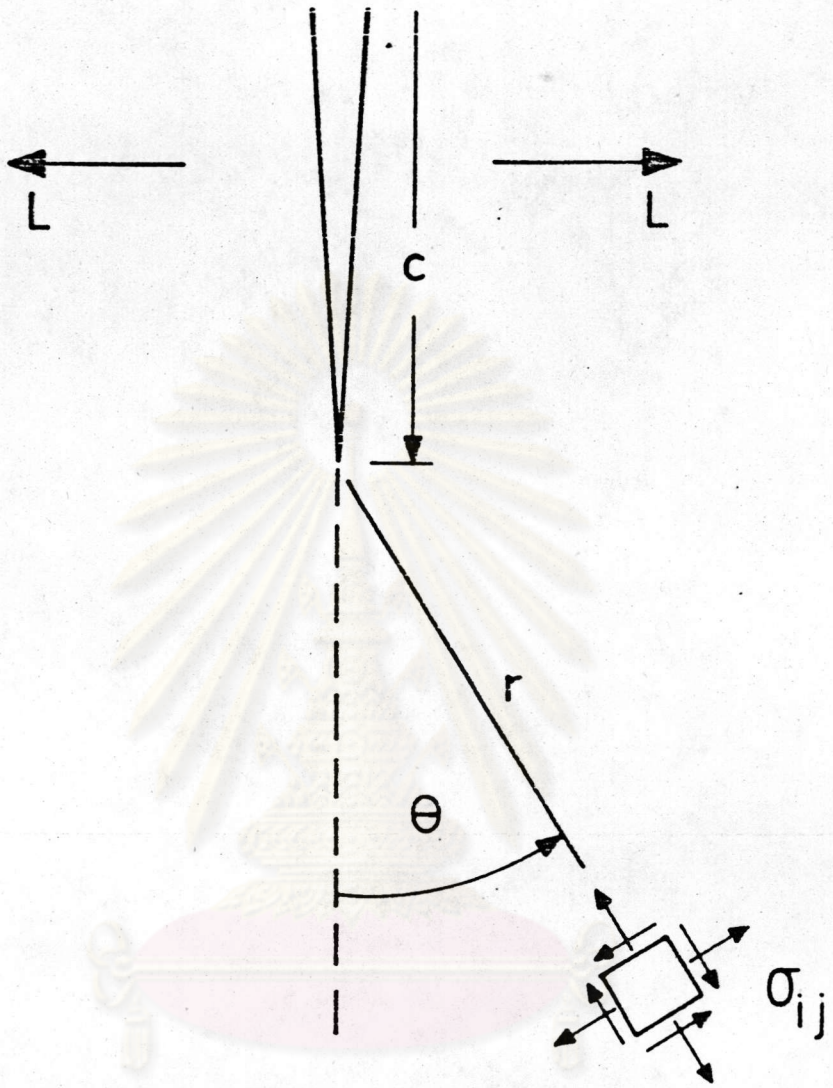

Fig. 3.1 Crack-tip fields. L and c respectively characterize the applied loading and scale of cracking.

The coordinate-dependent terms, fij (Θ) in Eq. (3.1) determine the distribution of the stresses within the field. The remaining factor K in Eq. (3.1) which is independent of the coordinates takes on a special significant. It depends only on the magnitude of the applied loading and crack geometry and thereby uniquely determine the intensity of the crack-tip stress field. This factor K, namely the stress intensity factor, is an extremely powerful parameter in general fracture mechanics analysis. It is a useful indicator of the crack driving force. Moreover, it follows from Eq. (3.1) that the stress intensity factors are additive, as the principle of superposition applied within the limit of linear elasticity theory. This additive property of K is of distinct advantage since stress intensity factors for superposed applied load states can add algebraically to give the net mechanical force on the fracture system.

The criteria which govern crack propagation of a given crack loading system can be formulated exclusively in terms of K. In cases where the crack-loading system is in high vacuum or inert environments, or at low temperature, equilibrium crack extension occurs when K associated with the given load and crack length exceeds some critical value K_c. Thus, K_c uniquely quantifies the resistance to crack growth and this quantity has now gained the widest acceptance as a material toughness parameter in engineering design. K_c can be related to the surface energy term via the Griffith criterion for equilibrium crack extension

$$K_c = [2\Gamma E / (1-\nu^2)]^{\frac{1}{2}} \qquad (3.2)$$

where Γ is the fracture surface crack energy, E Young's modulus, and ν Poisson's ratio.

In cases where the crack loading system is in a hostile chemical environment (e.g. water), cracks can extend at subcritical levels, $K < K_c$ Chemical processes activate bond-rupture at the crack tip and thereby advance the fracture at applied loads which would be insufficient to cause equilibrium crack extension in an inert environment. Accordingly, crack response to reactive environment and applied stress is rate controlled. The most widely used crack-velocity function which describes kinetic fracture is of the power-law type,

$$v = v_o(K/K_c)^n \quad , (K<K_c) \qquad (3.3)$$

Where v_o and n are constants depending on the given material / environment system.

3.1.2 Survey of Response of Various Materials to Vickers Indentation

In this section, we survey the different deformation / fracture damages occurring when glasses and ceramics are indented by a standard Vickers diamond pyramid indenter. Fig. 3.2 shows a typical Vickers fracture pattern which is visible on material surfaces as linear radial traces emanating from the corners of the indentation. The basic element of such damage pattern produced in Vickers indentation are well established (16). Around the sharp point of the pyramid contact the indented material deforms irreversibly, thereby

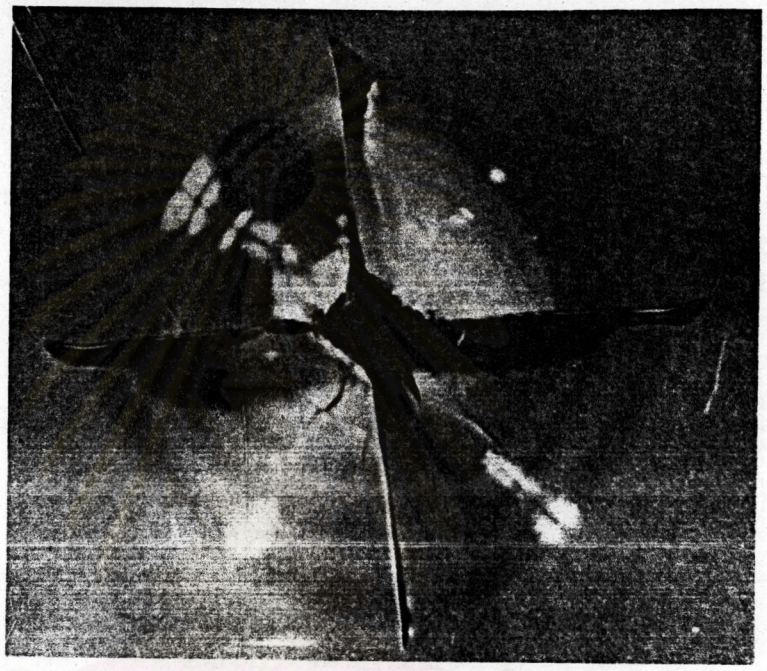

Fig. 3.2 Well - defined Vickers - produced crack (a) on the surface of glass showing linear radial traces emanating from the corners of the indentation (23),

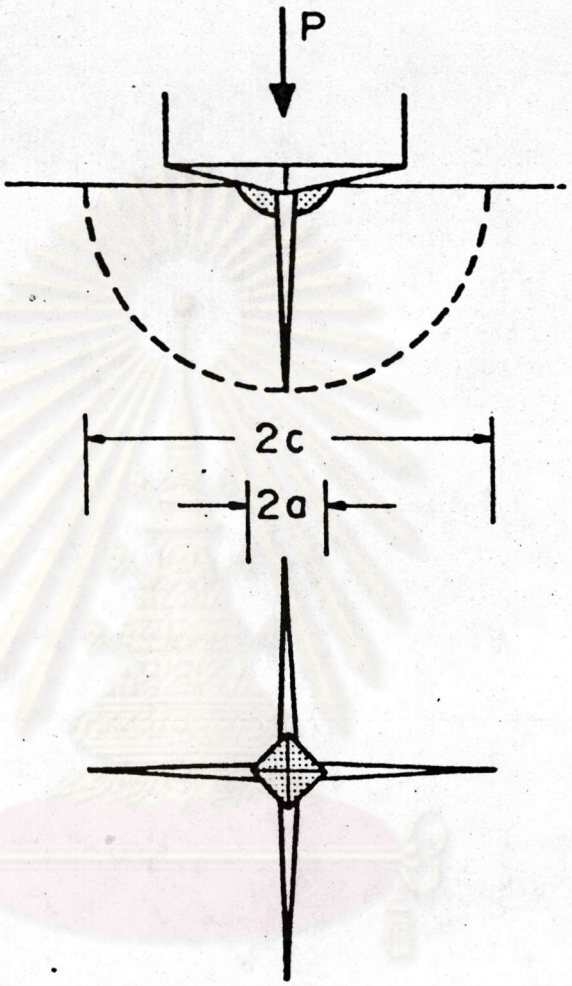

(b) showing the parameters of characteristic crack dimension 2c and the impression diagonal 2a.

creating a square impression. Emperically, it is found that the characteristic in-surface dimensions of the resultant impression, such as the impression half - diagonal a in Fig. 3.2 (b) remains a faithful indicator of the contact at maximum loading, thus justifying the use of post-indentation measurements to quantify the resistance to deformation. In this way we may define the material hardness in terms of the mean contact pressure,

$$H = P / 2a^2 \qquad (3.4)$$

where P is the peak contact load. Within the deformation zone crack nuclei are generated by the highly disruptive processes of structural rearrangement, and above some threshold load these nuclei become critical and propagate into the so-called "median" cracks contained on two orthogonal median planes each of which passes through the load axis and an impression diagonal. On further loading, median cracks grow stably downwards into penny-like shape. As unloading begins, the median cracks expand sideway and upwards to break through to the specimen surface, ultimately becoming near-semicircular in profile and is visible as radial traces extending from the impression corners. The manner in which the configuration develops from a contained sub-surface penny crack at full loading to a surface half-penny crack at full unloading can be seen from the half-section view micrograph in Fig. 3.3. This micrograph show fractographic features on the sodalime-glass specimen bein made to fail from one of the half-penny cracks after indentation.

Just prior to the full withdrawal of the indenter, an entirely new system, termed lateral cracks, begins to develop from nuclei within the deformation zone and spread laterally outward

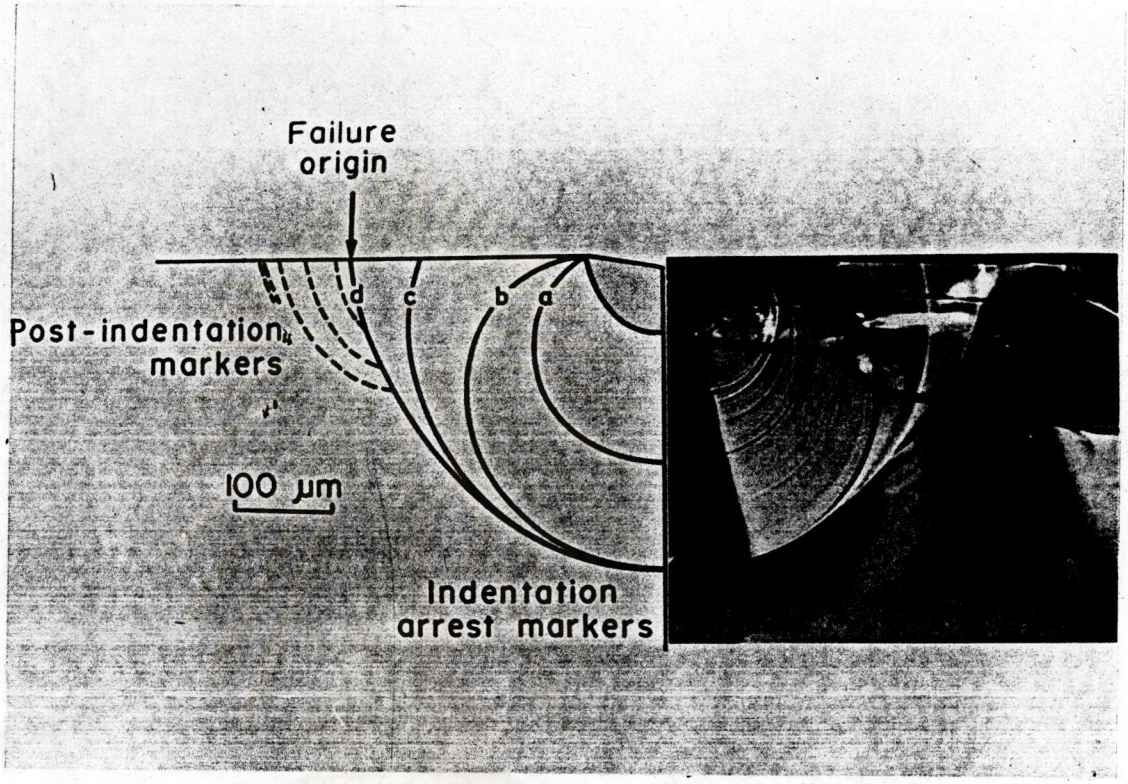

Fig. 3.3 Half-side view a half-schematic of median / radial crack system in soda-lime glass. Micrograph show fracture surface of specimen broken at indentation site crack-arrest markings are introduced to provide recorded crack evolution. Note failure origin at surface trace of half penny (23).

on planes closely parallel to the specimen surface in a saucer-like fashion as shown in Fig. 3.4. This crack can cause chipping if it intersects material surface, and is therefore particularly pertinent to the problems of surface wear and erosion. However, the lateral crack is not usually strength controlling crack and is accordingly given only minor consideration in this thesis.

Apart from the above mentioned subsurface crack geometry (the median / radial crack), there is another subsurface crack geometry associated with the four radial traces of the Vickers fracture pattern shown in Fig. 3.2. It is referred to as Palmqvist crack whose four independent subsurface cracks extend during loading radially along the median planes of the indentation into the dumb-bell shape closing to the specimen surface and on unloading these cracks grow both in length and in depth(Fig. 3.5).

The Palmqvist cracks have been extensively observed and studied in cemented carbides (17, 18). They are also observed in many ceramics, e g. zinc sulfide, zinc selenide and glass - ceramics (19, 20). A transition from Palmqvist cracks at low indentation loads to well - developed near semicircular crack at higher indentation loads was observed in zinc sulfide and zinc selenide whereas Vickers - produced cracks are still Palmqvist cracks even at high indentation loads in glass ceramics.

Fig. 3.6 shows another Vickers - produced damage observed in anomalous glass (21, 22). The dominant penetrative crack generated during loading resembles more a cone crack than a median crack. On unloading, there is a little change in the cone crack configuration. As unloading completes, a collar of material often

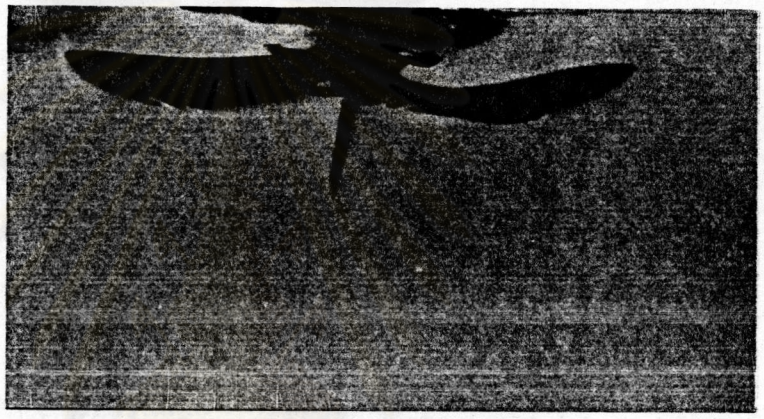

Fig 3.4 Side view of deformation/fracture pattern associated with Vickers pyramid indenter in glass showing the lateral crack spread sideways in saucer-like fashion toward the surface (23).

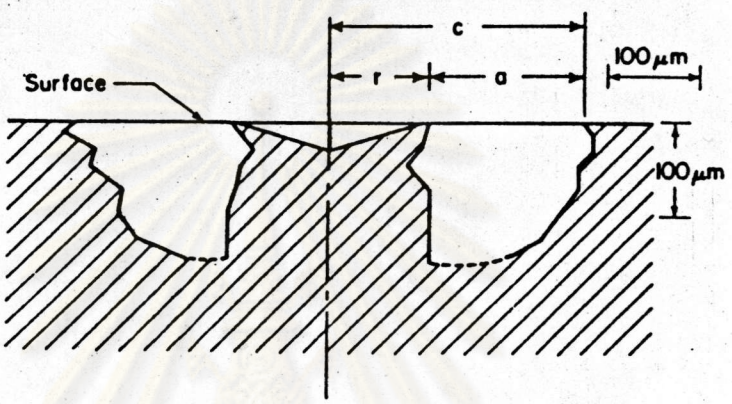

Fig. 3.5 Schematic of subsurface geometry of the Palmqvist cracks on median plane of a glass - ceramic (20).

Fig. 3.6 Profile view of cone - like indentation crack produced by Vickers diamond pyramid in partially leached glass (23).

detaches from part way down one or more of the cones to leave an annular surface crater , especially in heavily loaded surfaces.

From the broad survey given above, it can be seen that glasses and various ceramics have a variety of respones to Vickers indentations. Thus it is of importance to study the response of cattle bone material to Vickers indentations if the mechanics of formation of Vickers - produced damage in cattle bone material are to be understood. Such study, which will later be presented in this chapter, will provide considerable insight into the mechanics of formation of naturally occurring cracks which have surface contact history (see Sect. 1.2.2).

3.1.3 Mechanics of Vickers - Produced Cracks

The descriptions of the various Vickers - produced deformation / fracture process given in the previous sections are purely phenomenological. In this section we will outline their indentation fracture mechanics formulations. For the median / radial crack system, the corresponding stress distribution inside the indented materials are shown in Fig. 3.7 (16). Thus by virtue of the plastic contact the field driving the cracks contains both an elastic (reversible) and a residual (irreversible) component. Fig. 3.7 (b) shows stress contours of the elastic field in the median plane. Therefore during the loading half - cycle the tensile component of the elastic field enhances downwards crack extension but is constrained somewhat at the surface by the compressive component of the elastic field, thus cracks formed during the loading half - cycle is of penny shape. The residual component of the stress

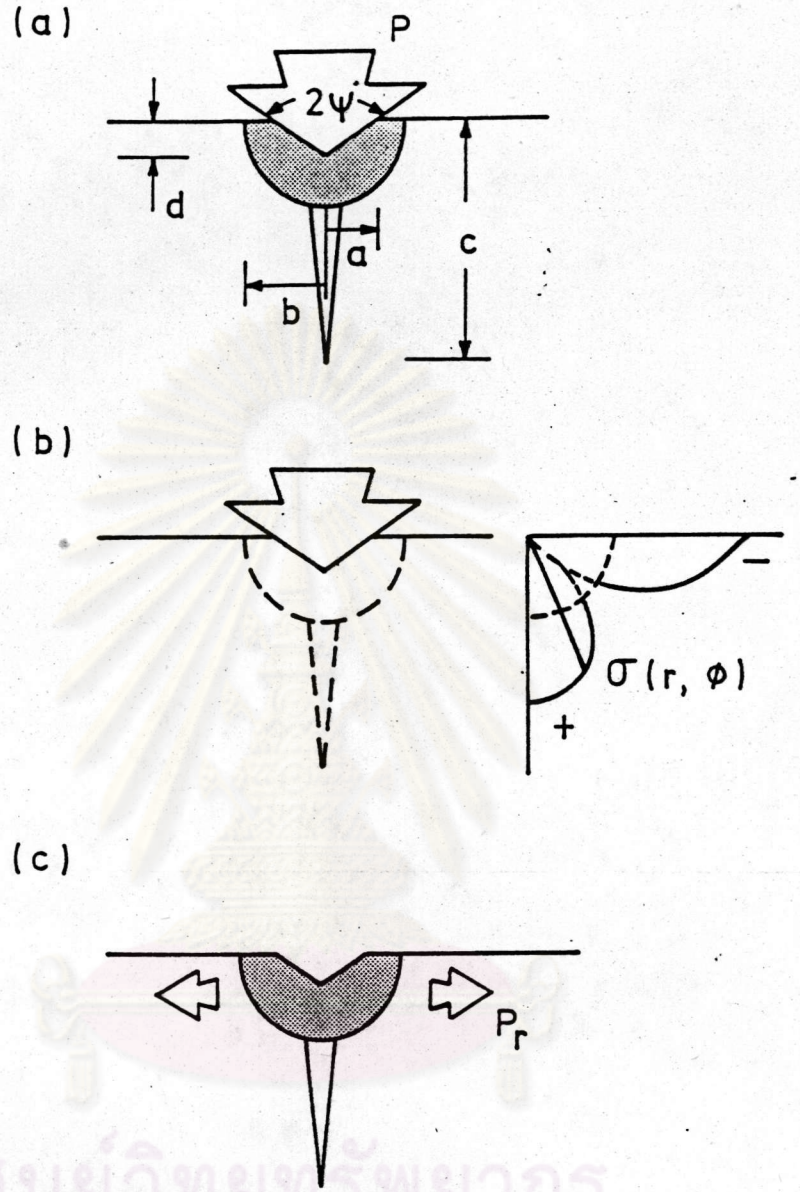

Fig. 3.7 Median/radial crack system, showing (a) elastic/plastic configuration at full load subdivided into (b) elastic component at full load plus (c) residual component at complete unload.

associated with stress / strain incompatibility between central deformation zone and surrounding elastic matrix and is characterized by a residual conter-opening force in Fig. 3.7 (c). Thus this residual field is superimposed on the tensile component of elastic field in driving downwards crack extension during the loading half-cycle. Accordingly, the stress intensity factor equation for the median crack which fully forms during the loading half-cycle can be written as (23)

$$K^M = (\chi_e^{M'} + \chi_r^M)\ P/c^{3/2} \qquad (3.5)$$

where χ_e^M and χ_r^M are the reversibility of the elastic term and the irrevesibility of residual term for the median component respectively.

During the unloading half-cycle, the compressive component of the elastic field is released, the residual field accordingly provides the primary driving force and the crack is thus driven radially outwards. Thus the stress intensity factor equation of the radial crack may be written as (10)

$$K^R = \chi_r^R\ P/c^{3/2} \qquad (3.6)$$

where χ_r^R is the irreversibility of residual term for the radial component and its magnitude depends on the ratio of (E/H) for different materials. Here E and H are Young's modulus and hardness of the material respectively. The radial crack were to persist in equilibrium after completion of the contact cycle, i.e. such that the requirement $K^R = K_c$ were to remain satisfied (see Sect. 3.1.1), then the fracture toughness paramater K_c of the material can be evaluated from the direct measurement of sizes of the equilibrium radial cracks, c_o, using the relation (10)

$$K_c = \zeta^R\ (E/H)^{1/2}\ (P/c_o^{3/2}) \qquad (3.7)$$

where χ_o^R is a nondimensional constant dependent only on the geometry of the indenter.

It is importance to note that the median crack closes up partially during the unloading half-cycle because of the reversible contact field on the completion of the indentation event, the radial crack remains fully open. Accordingly, the strength of materials containing a median / radial crack system is normally controlled by radial cracks. In addition, the fracture toughness K_c evaluated from direct crack measurements may be subjected to considerable errors if the system is exposed to a non-inert environment since the radial crack will continue to expand subcritically to $c_o' > c_o$.

For Palmqvist cracks, their length a (Fig. 3.5) has been shown to vary linearly with the indentation load P (17, 20, 24)

$$a = (P-P_o) / 4 W \qquad (3.8)$$

where P_o is a threshold indentation load for crack initiation and the constant W has been termed Palmqvist crack resistance (25) There have been many attempts in recent years to relate W to fracture toughness , K_c. . . The analyses predicted the following relation (26) :

$$K_c = \beta (HW)^{1/2} \qquad (3.9)$$

where the nondimensional constant β is a function of the elastic and plastic properties of the indented material

$$\beta = 0.025 (E/H)^{0.4} \qquad (3.10)$$

and H is the hardness of the indented material.

3.2 Experimental Procedure

In this section, we will investigate the response of the cattle bone material to the Vickers indentation. In order to be able to observe its deformation/fracture patterns produced by the Vickers indentation, the preexisting damages on specimen surface have to be removed by polishing with sucessively finer abrasive powders to obtain an optical finish. In this work, the optimum surface-removing procedure which did not introduce residual compressive stresses into the ultimate optical finish surface was found to be as follows:

(i) preliminary grinding with a series of SiC papers (800, 1000, 1200 mesh),

(ii) 60 min polishing with 9 and 5 μm alumina powders in a water slurry,

(iii) 30 min polishing with 2.5 and 1 μm diamond pastes.

When the polishing process was completed, the specimen was indented by a Vickers indenter at various indentation loads with the indents spaced far enough apart that no measurable crack interactions occurred. An Eseway microhardness tester was used to deliver loads within the range 10^{-1} to 10 N and an Eseway macrohardness tester at higher loads. During indentation, care was taken to maintain the indentation axis parallel to the surface normal of specimen.

After each indentation, the indented specimen was immediately transferred to the high magnification optical microscope in order to

examine the deformation / fracture pattern. The optical microscope was operated in reflected light since the cattle bone material was opaque to light in the visible region of the spectrum. Measurements of the dimensions of crack, c, and impression half-diagonal, a, were also immediately made. In addition, microscopic examination of section views of the indentation cracks (obtained by breaking the indented specimens at the indentation sites) was made to reveal the subsurface crack profile. Since the breaking surfaces of specimens were rough, a dye penetrant technique, in which the indented specimens were soaked overnight in methyl - orange solution before conducting the breaking tests, was used.

The indented specimen was also examined for evidence of post-indentation slow crack growth caused by environmental activated bond rupture at the crack tip (see Sect. 3.1.1). This was done by quickly transferring the newly indented specimens to the optical microscope and measured crack sizes as a function of time after completion of indentation loading cycle.

3.3 Results and Discussion

3.3.1 Damage Marphology

Optical micrographs of the Vickers damage pattern on surface of the cattle bone material indented with 10 N load is shown in Fig. 3.8. The damage pattern consist of a square residual contact impression of diagonal length, 2a, and four radial traces, c, extending from the corners of square impression. Surface chippings caused by another crack system, i.e. the lateral cracks (their

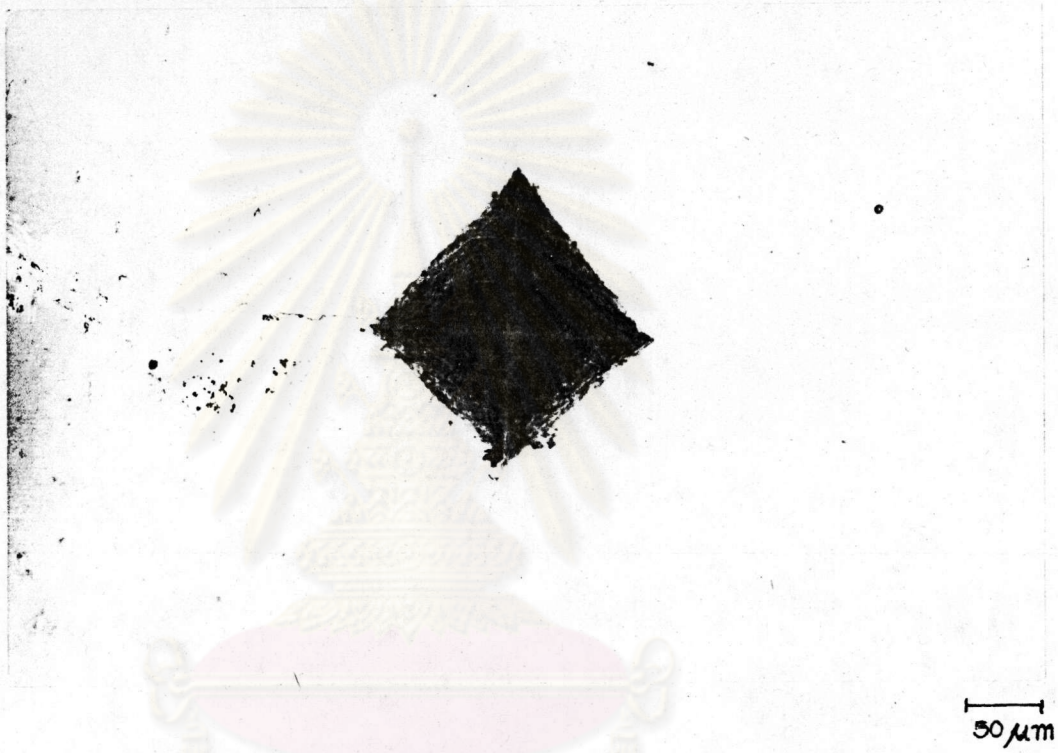

Fig. 3.8 Vickers - produced cracks on surface of the cattle bone material indented with 10 N, x 100.

occurrence will later be seen from the subsurface crack profile), were only observed when the indentation load were as high as 50 N (Fig. 3.9). At the indentation load above 100 N, the specimens failed spontaneously during indentation.

Optical micrograph of the subsurface crack profile of a specimen indented with 50 N load is illustrated in Fig. 3.10. Apart from the near-semicircular profile on the fracture surface the saucer-like traces which run nearly parallel to the specimen surface and centered beneath the contact zone, are also evident. Transition from Palmqvist cracks at low indentation loads to median / radial cracks at high indentation loads were not observed. Cracks remain of median / radial type at all load range. Thus it can be concluded from these photomicrographs that Vickers indentations produce two types of crack into the surface of cattle bone material : (i) the near-semicircular median / radial cracks forming on the two mutually orthogonal median planes of symmetry defined in each case by the indentation axis and one of the impression diagonals, centered on the contact point, (ii) the lateral cracks forming nearly parallel to the surface and centered beneath the contact zone. The lateral cracks are less penetrative than the median / radial crack. Accordingly these damage patterns of cattle bone material reflect the mechanics of formation of naturally occurring surface cracks which have surface contact history (see Sect. 1.2.2). In addition, the median / radial crack system which is more penetrative than the lateral crack system relates to strength properties of cattle bone material whereas the

Fig. 3,9 Surface chippings caused by the lateral cracks on cattle bone material (P = 50 N), x 50.

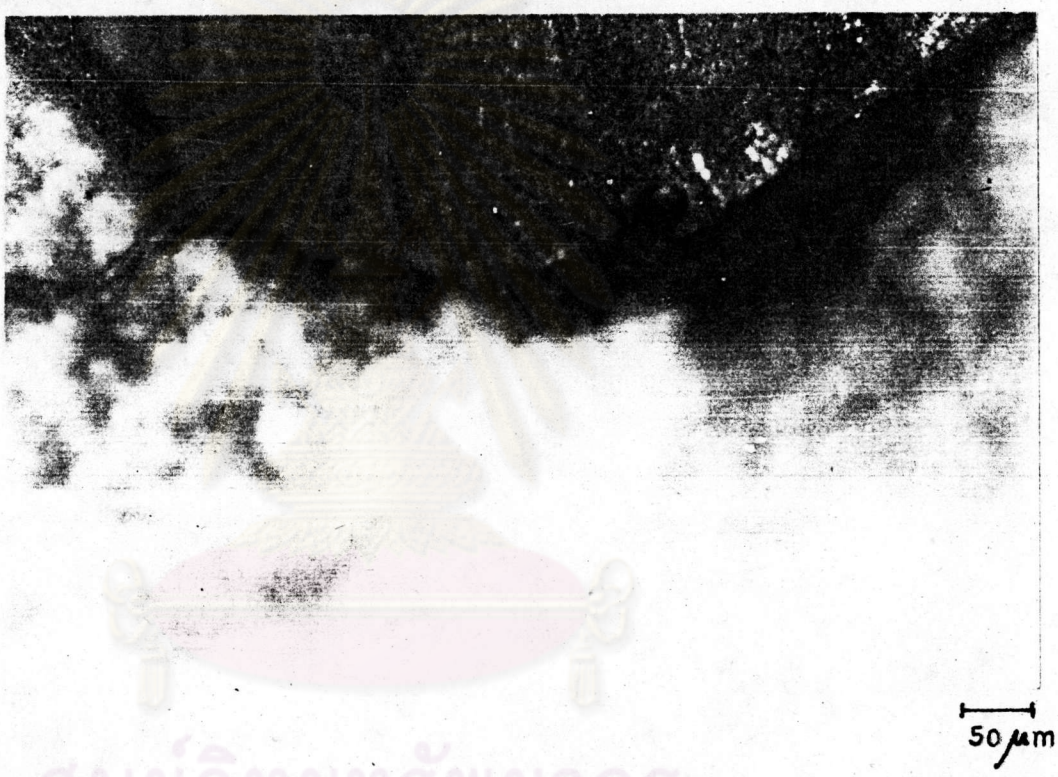

Fig. 3.10 The subsurface crack profile in the cattle bone material indented with 50 N, x 50.

lateral crack system which can deflect towards the surface and cause material removal relates to its surface wear and corrosion.

3.3.2 Indentation Load Dependence of Impression Half-Diagonal and Radial Crack Length

Dimensions of impressions half-diagonal, a, and radial crack length, c, measured from damage patterns such as that in Fig. 3.8 are plotted as a function of indentation load P in Figs. 3.11 and 3.12. Data were taken over as wide a range of indentation loads as possible, limited at lower loads by crack initiation and at higher loads by spontaneous failure during indentations. The dimension of impression half-diagonal for each indent was measured as averages over the two half-diagonals and the radial crack length as averages over the four radial traces. Each data point in Figs. 3.11 and 3.12 represents the mean and standard deviation of ten indentations. The results illustrated in Figs. 3.11 and 3.12 have established that the dimension of impression half-diogonal in cattle bone material follows the 1/2 power dependence of indentation load and the radial crack length follows the 2/3 power dependence of indentation load. Thus the above obtained dependences of a and c on P imply that Eqs. (3.4) and (3.7) are the equations to be used for evaluating hardness H and toughness K_c for the cattle bone material, respectively.Figs.3.13 and 3.14 resummarize the results of crack and impression half-diagonal measurments as plots of P/a^2 and $P/c^{3/2}$ as a function of indentation load P and the fitted lines are the means over all indentations. It can be seen from such plots that the mean values of P/a^2 = 1.87 GPa and $P/c_o^{3/2}$ = 8.20 MPa . $m^{1/2}$. From Eq. (3.4) along with the mean value of P/a^2, we obtain H = 0.93 GPa for cattle bone material. Using

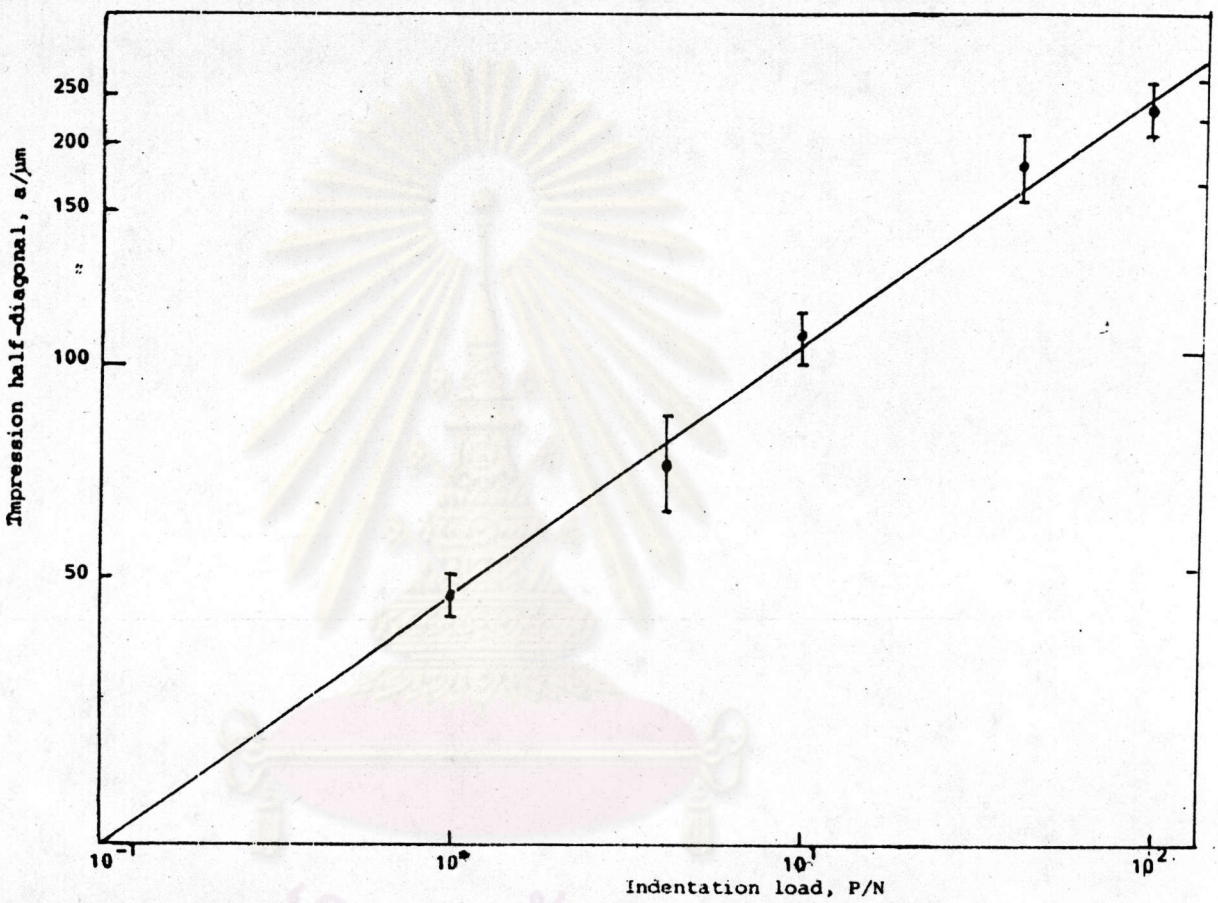

Fig. 3.11 Impression half - diagonal as a function of indentation load for the polished specimens. Error bars are standard deviations of 10 indentations.

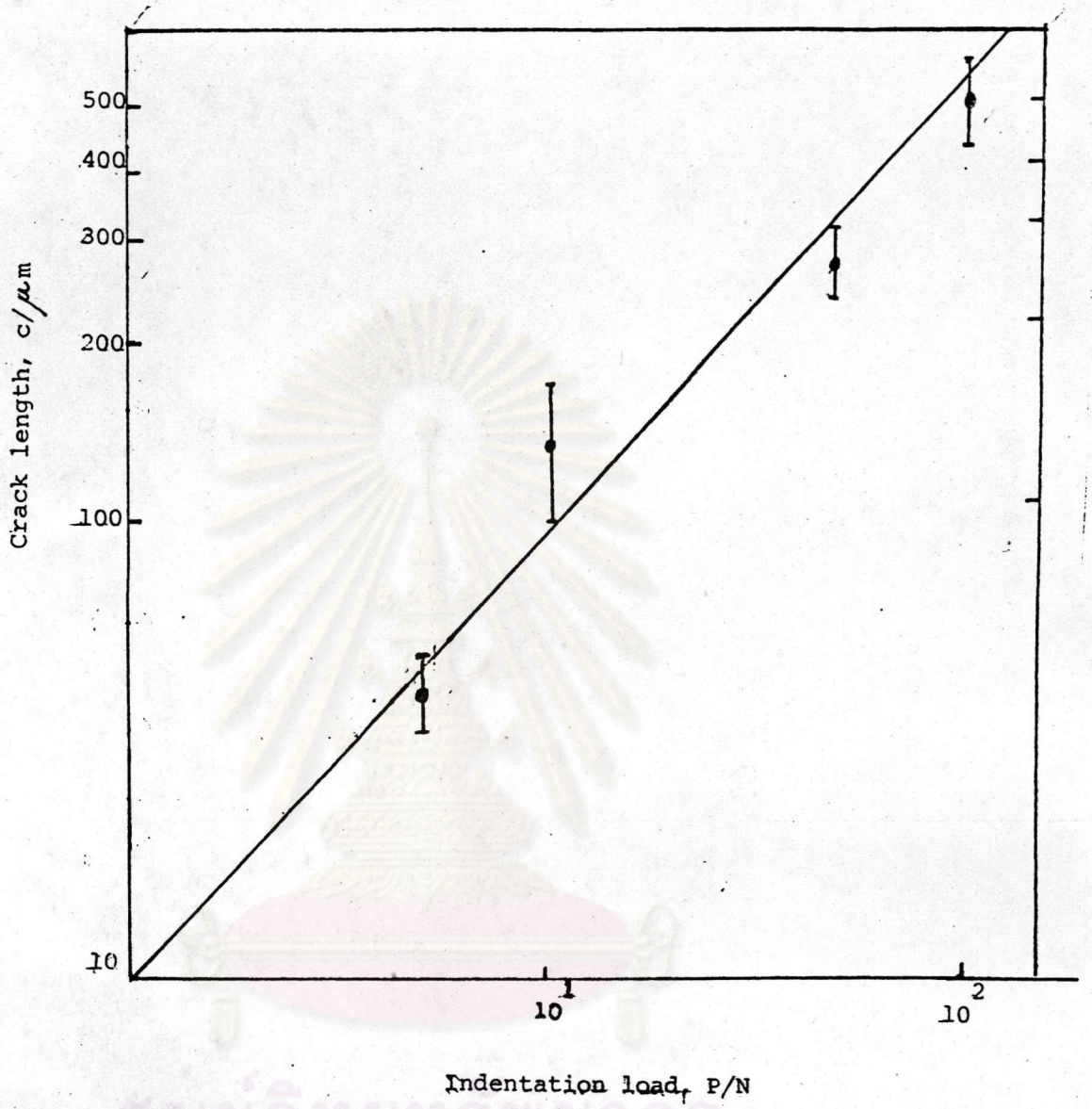

Fig. 3.12 Radial crack length as a function of indentation load.

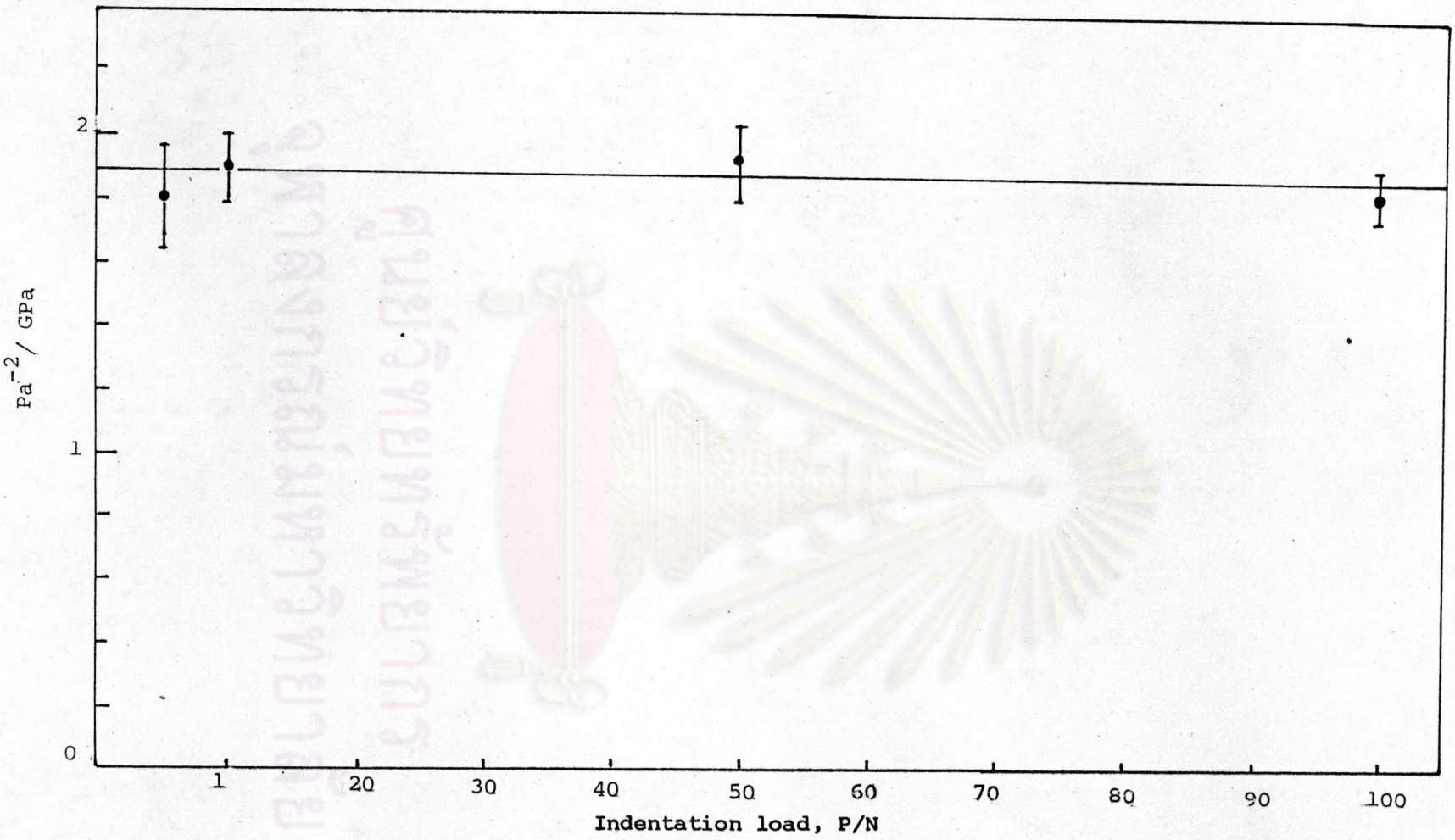

Fig. 3.13 Plot of Pa^{-2} over working range of load P. Error bars are standard deviations of 10 indentations.

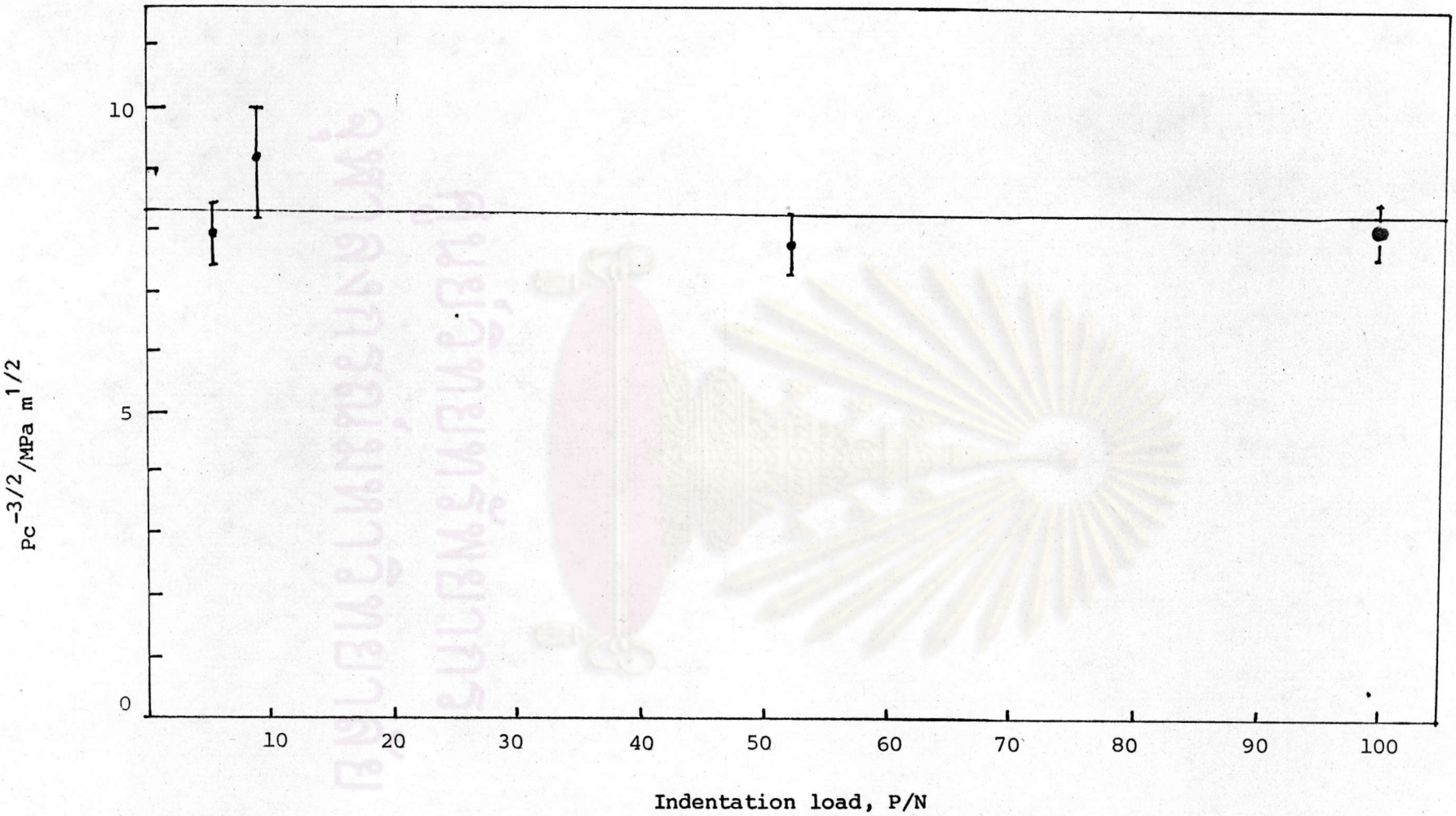

Fig. 3.14 Plot of $Pc^{-3/2}$ over working range of load P. Error bars are standard deviations of 10 indentations.

Eq. (3.7), K_c can be evaluated after replacing the values of ξ_0^R, E, H and $P/c_o^{3/2}$. For Vickers indenter, Antis et al. (10) established a value, $\xi_0^R = 0.016$, by calibrating indentation parameters with fracture toughness measured by conventional fracture mechanics techniques. Using Anstis et al. calibration value of ξ_0^R along with E = 0.30 GPa, H = 0.93 GPa and the mean value of $P/c_o^{3/2}$ yields $K_c = 0.07$ MPa. $m^{1/2}$ for cattle bone material.

3.3.3 Post-Indentation Slow Crack Growth

Dimensions of radial crack length c, measured as averages over the four radial traces are plotted as a function of time after completion of indentation loading cycle (Fig. 3.15). The result shows that there was a considerable extension of the newly formed indentation crack by slow crack growth from its initial crack size, c_o, as the time increasing and was effectively saturated at c_o' at the time which was more than two hours after the completion of the indentation event. The final crack size c_o' was almost two times of the equilibrium indentation crack size, c_o.

Such observed post-indentation slow crack growth show that the radial crack in cattle bone material is accompanied by the residual stress causing the radial crack to extend slowly in response to the moisture and the residual stress at subcritical stress level. In addition, this investigation demonstrates that in the analysis of indentation - controlled strength data of cattle bone material, which will later be made, the effect of residual stress needs to be taken into account. Furthermore, the measured radial crack sizes used in evaluating K_c of cattle bone material previously (Sect. 3.3.2) are

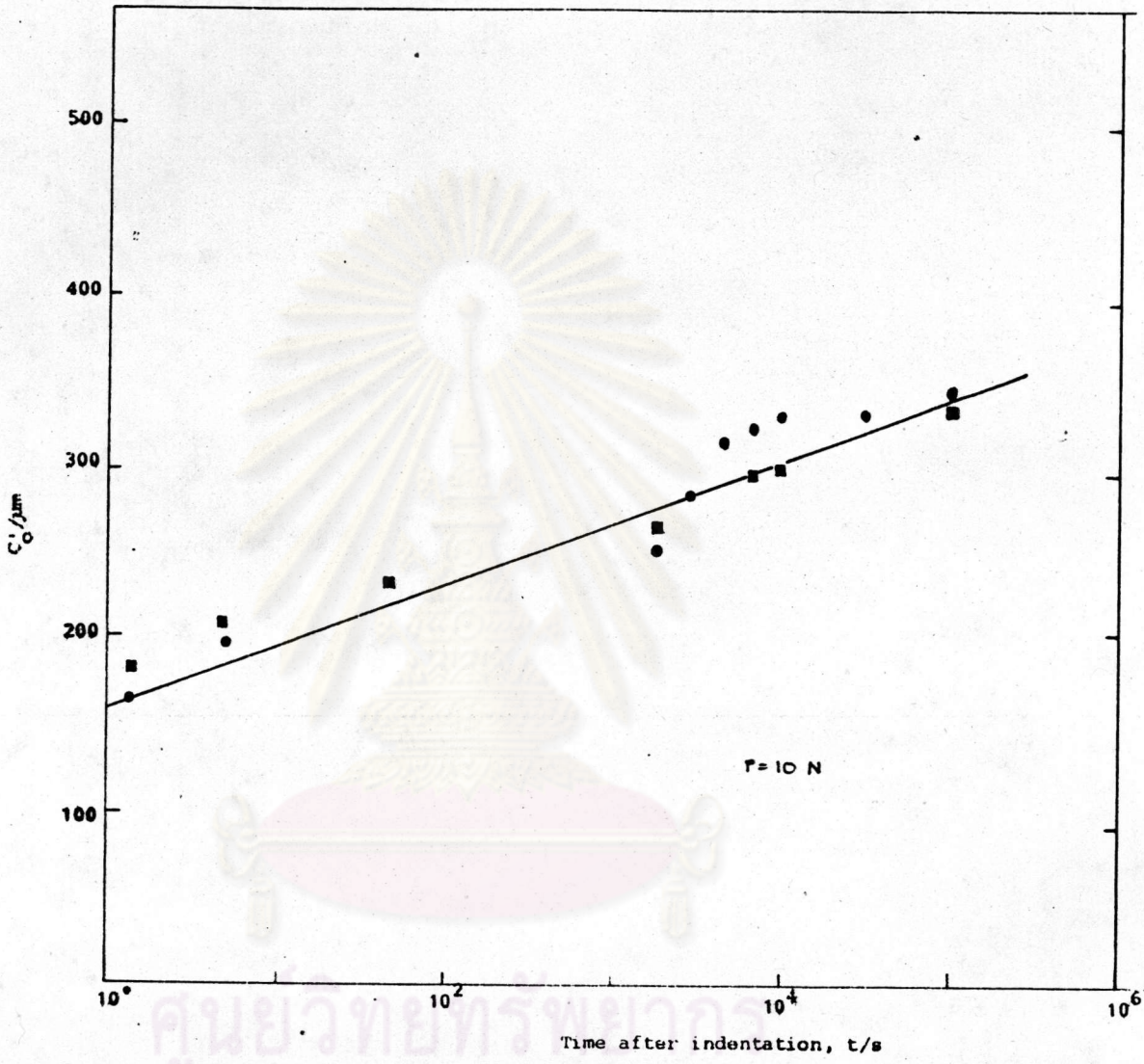

Fig. 3.15 Variation of radial crack length, c'_o, with time after indentation for tests in air environment.

not the true equilibrium crack size, c_o, therefore, K_c deduced from radial crack length measurements is subjected to considerable error due to the sensitivity of cattle bone material to post-indentation slow crack growth.